small methods
www.small-methods.com

Subtractive Patterning of Nanoscale Thin Films Using Acid-Based Electrohydrodynamic-Jet Printing

Tae H. Cho, Nazanin Farjam, Kira Barton, and Neil P. Dasgupta**

As an alternative to traditional photolithography, printing processes are widely explored for the patterning of customizable devices. However, to date, the majority of high-resolution printing processes for functional nanomaterials are additive in nature. To complement additive printing, there is a need for subtractive processes, where the printed ink results in material removal, rather than addition. In this study, a new subtractive patterning approach that uses electrohydrodynamic-jet (e-jet) printing of acid-based inks to etch nanoscale zinc oxide (ZnO) thin films deposited using atomic layer deposition (ALD) is introduced. By tuning the printing parameters, the depth and linewidth of the subtracted features can be tuned, with a minimum linewidth of 11 µm and a tunable channel depth with ≈5 nm resolution. Furthermore, by tuning the ink composition, the volatility and viscosity of the ink can be adjusted, resulting in variable spreading and dissolution dynamics at the solution/film interface. In the future, acid-based subtractive patterning using e-jet printing can be used for rapid prototyping or customizable manufacturing of functional devices on a range of substrates with nanoscale precision.

1. Introduction

Modern electronic devices require continuously increasing complexity and resolution, but currently, most devices are fabricated using photolithography. In contrast, additive manufacturing processes such as 3-D printing could enable customizable manufacturing of nanoelectronics, but most of these processes are limited by tradeoffs in throughput and spatial resolution, as well as a limited selection of available materials.[1–4] For instance, bottom-up nanomanufacturing processes such as scanning tunneling microscopy (STM) lithography and direct laser writing (DLW) techniques have trade-offs between throughput and cost, which limit the commercial applications of these processes.[1,5–8] Direct printing of materials, such as inkjet printing, often has strict limitations in the physical/chemical properties and composition of the ink material.[1,9] Furthermore, there is a growing demand to replace resource-intensive cleanroom processes with low-cost and scalable manufacturing methods for applications where device requirements are less stringent.

Electrohydrodynamic jet (e-jet) printing is an additive manufacturing technique that allows for fast and versatile patterning with high resolution. During e-jet printing, a jet of liquid ink is generated by applying an electric field between a conductive nozzle and substrate. This electric potential difference pulls the ink material out of the nozzle and drives fluid transport toward the substrate.[9–12] In e-jet printing, the ink is typically printed using conductive micro-capillary nozzles. At low voltages, the ink at the nozzle tip is at equilibrium with a spherical cap shape. As higher voltage is applied, the strong electric potential difference between the nozzle and the substrate deforms the ink from a spherical cap shape to a conical shape, the so-called "Taylor Cone", followed by the formation of a jet, which is thinner than the nozzle opening, from the nozzle toward the substrate.[9,11] As a result, e-jet printing can enable higher spatial resolution than traditional ink-jet printing (down to ≈10 nm), while maintaining reasonable print speeds (≈80 mm s^{-1}).[11,13] To date, e-jet printing has primarily been used to directly deposit materials onto the substrate surface using a variety of polymer and suspension-based inks.[12,9,14–20] Nozzle clogging due to the accumulation of the nanoparticles from solution-based inks at the nozzle tip is a challenge with e-jet printing. This results in strict requirements on the ink material that have limited the range of deposited materials, as well as the resulting printed material properties including chemical composition, microstructure, and defect content, which subsequently affect the functional properties of the printed layers.

To overcome the limitations of available ink materials, an alternative strategy to direct printing of functional materials is to

T. H. Cho, N. Farjam, K. Barton, N. P. Dasgupta
Department of Mechanical Engineering
University of Michigan
Ann Arbor, Michigan 48109, USA
E-mail: bartonkl@umich.edu; ndasgupt@umich.edu
K. Barton
Department of Robotics
University of Michigan
Ann Arbor, Michigan 48109, USA
N. P. Dasgupta
Department of Materials Science & Engineering
University of Michigan
Ann Arbor, Michigan 48109, USA

The ORCID identification number(s) for the author(s) of this article can be found under https://doi.org/10.1002/smtd.202301407

DOI: 10.1002/smtd.202301407

use the printed ink material to pattern layers that are deposited using a complementary process. In this strategy, the printed material is used to define a pattern, analogous to lithographic resist materials, while the functional material can be deposited by a variety of thin-film deposition processes.[21,22] For example, e-jet printing has been used to pattern thin films via lift-off, masked etching, and area-selective deposition.[9,23–27] However, lift-off-based processes are restricted in the thermal and chemical processing conditions of the overlying film, which must be compatible with the printed "resist" material. Alternatively, while printed features could be used as etch masks for subsequent wet or dry etch processes, the etch compatibility of the printed material restricts the processability. Furthermore, printed etch masks will only result in material removal in the unprinted regions, which is slow and prohibitive when the goal is to pattern small discrete features such as narrow lines or islands. Therefore, there is a need to complement the portfolio of additive printing processes with subtractive printing, where the printed ink directly displaces and/or removes the underlying substrate material.

Recently, we have introduced a new platform for additive nanomanufacturing that uses e-jet printing of polymer inhibitors to define regions for area-selective atomic layer deposition (ALD) with sub-μm resolution.[23] ALD was chosen as the thin-film deposition technique because of its versatile range of available materials (oxides, nitrides, sulfides, metals, etc.) with sub-nm precision in film thickness and composition, while also maintaining uniform and conformal deposition at relatively low temperatures (< 250 °C).[28–31] By combining the sub-nm resolution of ALD in the z-direction with the sub-μm resolution of e-jet in the x-y plane, additive nanomanufacturing of functional materials can be performed with customizable patterns and high spatial resolution. Using this approach, thin film transistors were fabricated, demonstrating the potential for this platform to enable printable electronics with customizable feature dimensions and diverse material compositions.

To date, most of the previous works using inkjet and/or e-jet printing to pattern functional devices by ALD have involved area-selective ALD (AS-ALD), where the printed polymer pattern defines the regions where subsequent ALD deposition does not occur.[21–23] Previously, we have introduced a new approach for subtractive patterning of polymer inhibitor layers using solvent inks, which exposed the underlying surface for subsequent AS-ALD deposition.[32] However, AS-ALD is limited by an imperfect selectivity window, as well as potentially undesirable effects from vapor phase infiltration of the ALD precursors into the printed polymer layers.[33–36] Furthermore, processes where thin-film deposition occurs after printing the polymer patterns are limited by the thermal and chemical stability window of the printed polymer materials. As an alternative to AS-ALD, direct-write ALD processes have also been reported using atomic-layer additive manufacturing (ALAM).[37,38] An advantage of this technique is that it allows for selective deposition of ALD materials, without any pre/post patterning steps. However, the lateral resolution of the pattern is defined by microfluidic gas channels for precursor delivery (≈300 μm), which could be challenging to implement if higher x-y resolution is required. Therefore, there is a need for new subtractive printing approaches that can selectively remove the underlying deposited layers, which alleviates many of these processing constraints.

In this study, we demonstrate an alternative strategy for subtractive e-jet printing of nanoscale thin films, without the need for patterning of a polymer resist layer. In this approach, we use an acid-based ink [hydrochloric acid (HCl) mixed with glycerol] to directly pattern an underlying ALD film (**Scheme 1**). The deposited ink reacts with the underlying ALD material, resulting in etching and dissolution of the film material into the printed polymer pattern (Scheme 1b). Finally, the residual polymer composite that remains on the surface after printing is removed by rinsing with water, resulting in the formation of an etched surface feature with the linewidth of the printed layer (Scheme 1c). We further show that by varying the number of printed layers, the geometry of the resulting geometry can be tuned with nanometer resolution in the z-direction and micrometer resolution in the x-y plane. Finally, the influence of ink composition on the spreading, wetting, and dissolution behavior at the solution/film interface is described. In the future, subtractive patterning of ALD films using e-jet printing can expand upon the existing toolbox of additive nanomanufacturing processes for customizable device fabrication.

2. Results and Discussion

As described in the introduction, the goal of this study is to use e-jet printing for subtractive patterning of nanoscale thin films. As a model material system, we focused on ZnO films grown by ALD owing to their favorable properties including facile self-limiting ALD growth, diverse functional properties (optical transparency, tunable electrical conductivity, etc.), and a broad range of application uses (thin film electronics, photocatalysis, sensors, etc.).[39–41] Furthermore, ZnO is known to etch easily in acidic solutions, making it favorable as a model system to study subtractive patterning.[42,43]

Our initial attempts to pattern ZnO with e-jet printing employed a pure aqueous HCl solution as the ink. However, it was observed that the ink would easily dry out when printed on the surface. The printed ink also coalesced into small isolated droplets due to a larger cohesion force than adhesion force (Video S1, Supporting Information). This nonideal patterning behavior is attributed to the extremely small volume of the ejected ink that is characteristic of high-resolution e-jet printing (in the range of fL), along with the relatively high vapor pressure of the aqueous HCl solution, which results in nearly instantaneous evaporation when the ink contacts with the substrate surface (in situ visualization of the aqueous HCl ink printing process is provided in Video S1, Supporting Information).[44] If the ink evaporation takes place faster than the etching reaction, only the very top layer of ZnO is removed. To characterize the resulting changes to the film surface, atomic force microscopy (AFM) analysis was performed after printing with a 1 M HCl ink, and minimal changes in topology were observed. This provides evidence that pure aqueous HCl inks do not allow enough time for the etching reaction to occur with the underlying bulk metal oxide. Moreover, the high conductivity of the HCl solution leads to an unstable Taylor Cone, resulting in a non-robust/unreliable printing process.[46]

To overcome these limitations and control the evaporation rate of the ink, a small amount of glycerol (1-2 wt.%) was mixed into the 1 M HCl solution. Glycerol was chosen as a non-volatile

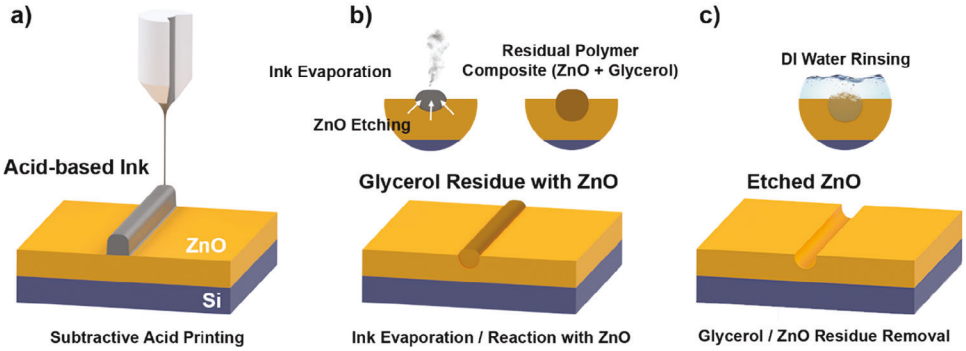

Scheme 1. Process flow of subtractive e-jet printing using an acid-based ink. a) Acid-based ink is printed on ZnO film surface using e-jet b) As the ink evaporates, the aqueous HCl component reacts with the ZnO to form a residual polymer composite (ZnO + glycerol) c) When rinsing in DI water, the residual polymer composite gets removed which leaves an etched trench of ZnO behind.

dilutant that lowers the vapor pressure of the ink solution, thereby reducing the evaporation rate.[46] Adding glycerol also increases the ink viscosity, resulting in a slower jet that is easier to control during the process (in situ visualization of the glycerol-ink printing process is provided in Video S2, Supporting Information).[46,47] Moreover, adding glycerol decreases the conductivity of the ink material, resulting in a more stable jetting behavior. When the glycerol-HCl ink mixture is printed on the surface, the acidic solution remains on the surface for a sufficiently long time to etch the underlying ZnO film. Subsequently, as the water evaporates from the printed ink, the glycerol solidifies to form a polymer composite containing the dissolved Zn atoms, as illustrated in Scheme 1.

To demonstrate the feasibility of this approach, a series of lines were printed and analyzed using optical microscopy (**Figure 1**). As we have previously demonstrated for subtractive printing of polymer films using solvent inks, the linewidth and depth of the printed geometry depend on a number of factors, including ejected material volume, number of printed layers, and surface energy of the material being dissolved.[32] By increasing the number of printed layers while maintaining a small ejected material volume, the etched material depth can be tuned without significant increases in linewidth, which enables subtractive patterning of high-aspect-ratio trenches. Therefore, in this study, an optimal ejected material volume that enabled etching before complete evaporation of the water content was first identified, and the etched depth was then controlled by varying the number of printed layers.

Figure 1a shows a series of lines where the number of printed layers was systematically varied. Figure 1b shows that after glycerol removal, the etched trenches in the ZnO film are exposed, as illustrated in Scheme 1. In e-jet printing, the printed material topography is influenced by a number of variables including droplet ejection, spreading, and evaporation/coalescence dynamics, which are specific to the ink and substrate material systems.[9,11] When a sufficient number of layers were printed (> 30 layers), a continuous line of residual polymer composite was observed. However, when fewer layers were printed (e.g., 10–20 layers), the residual polymer composite that remained on the surface after ink evaporation formed a discontinuous line. Despite these differences in the morphology of the residual polymer composite, after the removal of the solid residue with DI water, the etched trenches that remained on the surface always formed continuous lines (Figure 1b).

To rationalize this behavior, we must consider the dynamics of the liquid-to-solid phase transformation that occurs as the aqueous component of the ink evaporates. Because the etching process occurs at the liquid ink/ZnO interface, the trench geometry is determined by the initial contact between the printed ink and substrate, which forms in a continuous line because of the linear motion of the stage relative to the printer nozzle. However, as the ink evaporates, a phase transformation to solid occurs as the residual polymer composite forms. The final topology of the remaining solid phase will be strongly affected by the dynamics of this evaporation and coalescence process. In particular, as liquid evaporation occurs, the wetting behavior of the remaining solid

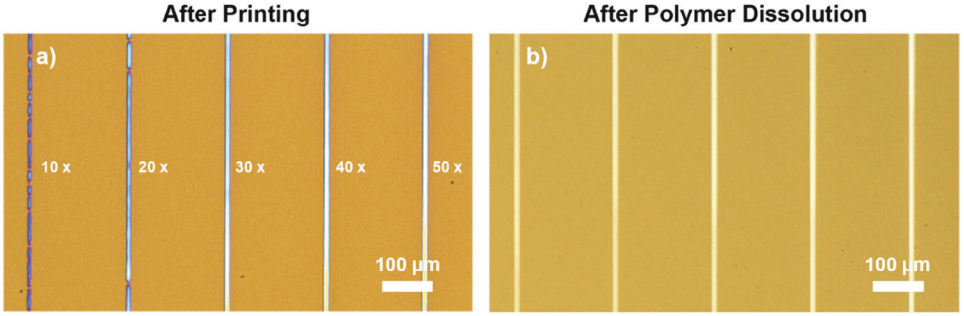

Figure 1. Optical microscopy images of printed ZnO (a) before glycerol removal, and b) after glycerol removal with different numbers of printed layers.

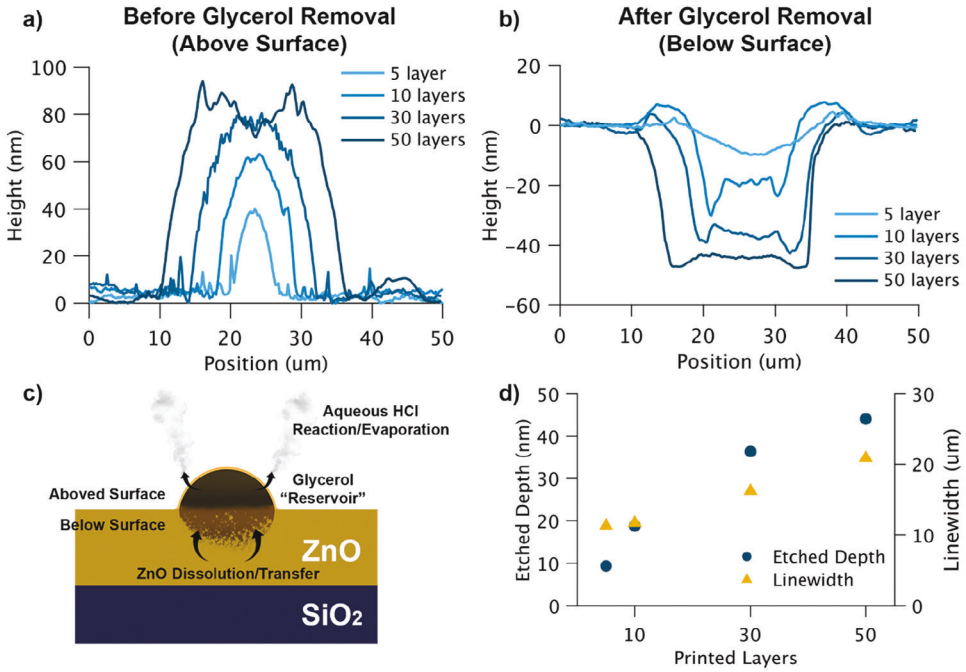

Figure 2. AFM scans after e-jet printing a) before glycerol removal (above the surface), and b) after glycerol removal (below the surface) with a varying number of printed layers. c) Schematic showing the simultaneous etching and evaporation processes, resulting in a residual polymer composite that "stores" the etched Zn atoms. d) Quantification of etched material depth (average within base region) and linewidth (full width at half maximum) as a function of the number of printed layers

on the surface will evolve based on the thermodynamic balance of surface, bulk, and interfacial energies, as described by classical wetting theory through Young's equation. As a result, the merging behavior of the deposited ink materials will be influenced by the contact angle, which may result in droplets separating from each other.[46] Furthermore, the kinetics of evaporation can also affect the final topology, as the final solid morphology may become "frozen" in place as the viscosity of the remaining liquid increases during evaporation. Because etching only occurs when the aqueous (liquid) component of the ink is in direct contact with the underlying ZnO film, the dynamics of polymer coalescence near the end of evaporation do not have a strong correlation to the etched trench geometry.

By varying the number of printed layers, the resulting depth of the etched trenches can be controlled. To observe the effects of the total number of printed layers on the displaced depth and linewidth, AFM scans were conducted before and after glycerol removal. When sequential layers of ink are printed on a ZnO surface, the height and linewidth of the residual polymer composite above the film surface both increase (**Figure 2a**). After printing 5 layers, the height of the resulting polymer composite was ≈38 nm and the linewidth (full width at half maximum) was ≈5 µm. As the number of printed layers increased, the linewidth was observed to increase monotonically, while the height of the printed polymer composite reached a plateau of ≈83 nm after 50 layers.

When 50 layers were printed, the top surface of the polymer composite residue started to form a "trough" in the middle, with the height of the outer edges of the printed line being slightly larger than in the middle. This behavior can be rationalized based on our previous observations of subtractive e-jet printing of PMMA polymers using solvent inks. Because the residual polymer composite is soluble in the aqueous ink printed in subsequent cycles, when the printed polymer composite becomes sufficiently thick, lateral displacement of the solid material toward the outer edges of the printed lines can occur as a result of the "coffee ring" effect during ink evaporation.[32] In this case, the residual polymer composite from previous layers is displaced, rather than etched by the newly printed layers on top, resulting in the observed trench morphology after ink evaporation.

After the residual polymer composite is rinsed with DI water, the subsurface trench that was formed during etching is exposed, completing the subtractive patterning process. These etched trench geometries were then analyzed using AFM. Analogous to the trends in the residual polymer composite before rinsing, as the total number of printed layers increases, the resulting depth and linewidth of the etched trenches also increase (Figure 2d). After 50 layers of printing, the maximum etched depth reached ~50 nm, which was equal to the total deposited ZnO film thickness.

A summary of the dynamic processes that occur during the subtractive patterning process is illustrated schematically in Figure 2c. As each layer of ink is printed, the subsurface geometry of the residual composite deepens as a result of the ZnO film being etched. Because the etching process only occurs while the ink is in the liquid phase, the volume of the ink droplets on the surface determines the evaporation rate (and thus the total time of the etching reaction). Once the liquid evaporates, the etching process self-terminates. As we will show later, the etched Zn atoms are incorporated into the residual polymer composite that forms as the aqueous component of the ink evaporates. Therefore, the

detailed evolution of the subsurface geometry will depend on the dynamic evolution of the ink/substrate interactions of ZnO during these concurrent etching and evaporation processes.

For a single layer of printed ink, the etched depth will be determined by the competing rates of the etching and evaporation processes, resulting in a shallow and narrow trench. As subsequent layers are printed, the aqueous HCl content within the printed glycerol region is replenished, resulting in additional etching of ZnO before the next evaporation process is complete. In this sense, the glycerol is acting as a "reservoir" for HCl storage during the etching process by modulating the evaporation rate. As each additional layer is printed, the total volume of the residual composite increases, which causes an increase in the linewidth of the etched trench (Figure 2b) as well as an increase in the height and linewidth of the residual composite above the surface of the film (Figure 2a). We further note that in Figure 2d, the incremental etching depth per layer decreases as more layers are printed. This can be rationalized by the fact that the volume of the residual polymer that remains on the surface after ink evaporation continually increases as more layers are printed (Figure 2a). Therefore, the "reservoir" into which the liquid ink is absorbed (and is transported to the film/residual polymer interface) increases with increasing cycle numbers. As a result, the transport of the liquid ink to the surface slows down as the volume of residual polymer composite increases each cycle (as quantified by AFM in Figure 2a).

In summary, the dynamic evolution of the etched geometry will depend upon the concurrent processes (e.g., dissolution, evaporation, accumulation) during subtractive patterning of thin films using acid-based inks. To control these processes, a number of variables can be tuned, including ink composition, printing parameters (printing speed, voltage, pulse width, etc.), and ink-surface interactions (e.g., wetting and surface energy effects).

As an example of tuning one of these process parameters, the weight percentage of glycerol in ink solution was varied from 1%–2%. This range was chosen because inks containing > 2 wt.% of glycerol resulted in poor wetting of the substrate, which will lead to nonuniform etching behavior. As shown in Figure 2b, when 50 layers were printed on the ZnO surface using the 2 wt. % glycerol ink, the resulting trench depth was ≈50 nm, with a nearly rectangular cross-section. When fewer layers were printed, a slight wave-like cross-section can be observed, resulting in a channel topology with an elevated central peak surrounded by two recessed valleys. This is analogous to observations from solvent-based subtractive patterning using e-jet printing, where this topology was attributed to Marangoni flow as the ink droplet evaporates from the surface.[32] Marangoni flow is driven by a nonuniform surface tension gradient along the droplet-free surface originating from a non-uniform evaporation rate, which induces an inward flow inside the droplet resulting in wave-like etching behavior, as illustrated schematically in **Figure 3**b.[48,49] However, when a 2 wt.% ink was used, the effects of Marangoni flow were relatively minimal, and after 50 layers of printing, the base of the cross-section was nearly flat, illustrating complete etching of the film without a central peak of ZnO remaining (Figure 2b).

When 1 wt.% ink was printed, the effects of Marangoni flow became more prominent, as shown in Figure 3. The changes in Marangoni flow behavior as a function of ink composition will

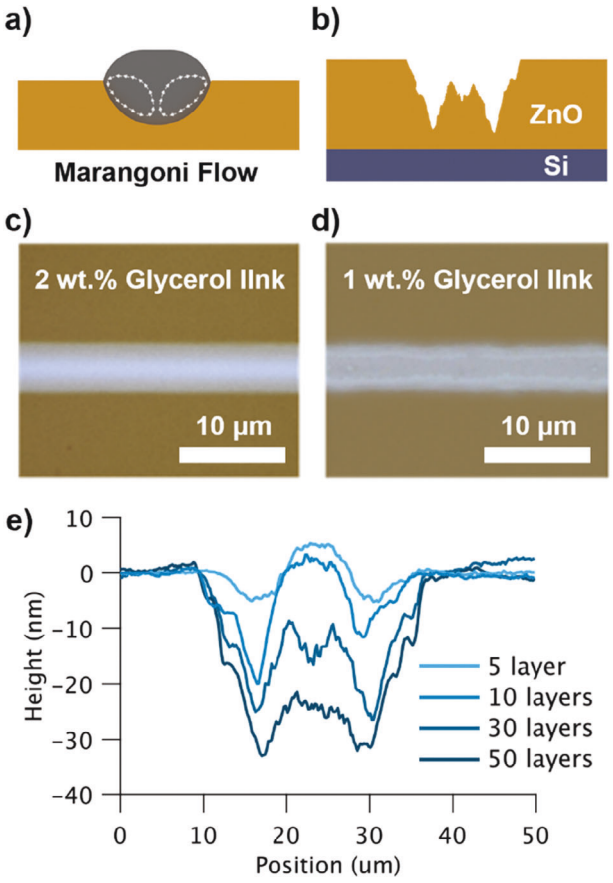

Figure 3. Schematic showing a) Marangoni flow and b) resulting cross-sectional geometry of Marangoni flow after acid-based subtractive printing. Optical microscopy images of subtractive-patterned ZnO surface using HCl ink mixed with c) 2 wt. % and d) 1 wt. % of glycerol ink. e) AFM scan of ZnO surface after printing 1 wt. % glycerol ink and rinsing to remove the residual polymer composite.

be influenced by the changes in the ink viscosity and evaporation, resulting in the observed differences in the cross-sectional profile.[48,49] In addition to the change in cross-section shape, the overall etched depth was shallower, which is also consistent with the faster evaporation rate of the aqueous HCl component of the ink. Overall, these results demonstrate the importance of tuning the ink composition when controlling subtractive patterning processes.

Another notable aspect of the cross-sectional profile of the etched feature was the absence of side rims. In our previous work on solvent-based subtractive printing of polymers, the polymer material was displaced toward the edge of the printed line as the solvent ink evaporated, leaving tall side rims.[32] However, only minimal side rims were observed for acid-based subtractive printing of ZnO in Figures 2 and 3. The difference between acid-based subtractive printing and solvent-based subtractive printing is the addition of glycerol in the ink. In solvent-based processes, once the ink evaporates, the dissolved polymer material resolidifies on the surface. In contrast, when HCl-glycerol solution inks are used, the etched Zn atoms are incorporated into the residual polymer composite that remains on the surface after

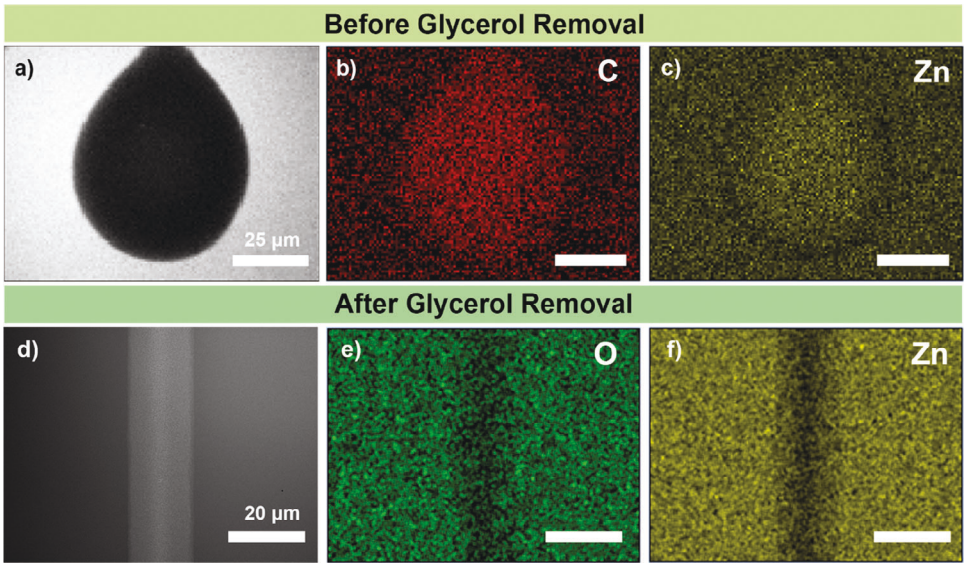

Figure 4. Subtractive printing of ZnO using acid-based e-jet: (a) SEM image of the printed pattern before polymer removal and b,c) C and Zn EDS map scan; (d) SEM image of the printed line after polymer removal in DI water and e,f) O and Zn EDS map scan of etched ZnO trench, respectively.

the aqueous HCl component evaporates, as will be shown in the following section. During the subsequent dissolution process in water, the etched Zn material is washed away with the residue, and therefore the etched material is completely removed.

To study the chemical composition of the residual polymer composite after acid-based printing and before the final DI water rinsing step, scanning electron microscopy (SEM) – energy dispersive spectroscopy (EDS) analysis was performed (**Figure 4**). The sample with 50 layers of printing was imaged, which resulted in the etching of the entire 50 nm ALD ZnO film after the residual polymer composite was removed (Figure 2b). C, O, and Zn were mapped on the printed surface before and after polymer removal. High concentrations of C and Zn were observed in the printed region (before rinsing), which demonstrates that etched Zn atoms remain within the glycerol residue region after printing (Figure 4a–c). After the residual polymer composite was removed by rinsing in DI water, no Zn and O were observed (Figure 4d-f), demonstrating that the original ZnO film had been completely removed with the glycerol. Furthermore, no noticeable concentration of C was detected after glycerol removal (Figure S3, Supporting Information). Together, these results demonstrate that the initial printing process results in the etching of the ZnO film and incorporation of Zn into the residual polymer composite, which is subsequently removed by DI water rinsing, as illustrated in Scheme 1 above.

To provide further quantification of the etched Zn atoms that are incorporated into the residual polymer composite during acid-based printing, inductively coupled plasma mass spectrometry (ICP-MS) was performed after dissolving the polymer composite in DI water (Table S1, Supporting Information). To measure the Zn content within the residual polymer composite, 1 µL of 1 M HCl + 2 wt.% glycerol ink was dropped using a micropipette on 50 nm ZnO and was left for 72 h for the ink to completely evaporate. After dissolving the glycerol residue in 1 mL of DI water, 17.71 ppm of Zn was measured, showing that the glycerol residue contains Zn, which is consistent with the SEM-EDS results in Figure 4. This is also in reasonable agreement with the droplet size of the ink on the substrate (further details in Supporting Information). These observations support the mechanism depicted in Scheme 1, where subtractive printing can be performed using ink mixtures that concurrently dissolve and store atoms from the underlying material, which can be subsequently removed during rinsing.

3. Conclusion

In this work, we demonstrated subtractive patterning of ZnO thin films using e-jet printing with acid-based inks. An aqueous mixture of HCl mixed with glycerol was used as the etchant ink, and an optimal concentration of 2 wt.% glycerol was found to provide the ideal balance between the evaporation rate and Marangoni flow behavior, resulting in etched trenches with an approximately rectangular cross-sectional profile. The etched material width and depth could be controlled by varying the number of printed layers, with a minimum linewidth of ≈11 µm and a tunable depth resolution of ≈5 nm. The mechanism of this subtractive patterning process was shown to consist of etching of the underlying ZnO substrate by the acid component in the ink mixture, which results in the incorporation of Zn atoms into the residual polymer composite that remains on the surface after the aqueous component evaporates. To provide evidence for this mechanism, SEM-EDS mapping and ICP-MS analysis were performed, which showed the presence of Zn in the residual polymer composite. This residual polymer composite can be subsequently rinsed in DI water, resulting in the removal of Zn atoms from the printed region.

In the future, the method developed in this study for subtractive printing can be extended to additional material systems, where the ink composition can be tuned to control the etching and evaporation rates. For example, wet etching processes exist for a variety of metal oxides, nitrides, and sulfides (ex. Cu_xO, SnO_2, and AlN), which can be performed using acidic or basic

solutions that are compatible with e-jet inks.[50,51] Furthermore, by combining subtractive printing using e-jet patterning with precise and tunable thin-film deposition methods such as ALD, nanomanufacturing of complex 3-D architectures with precise control of spatial variations in composition and thickness can be realized (Figure S4, Supporting Information). The processes described herein can be potentially extended to different substrates and form factors, enabling future applications ranging from printable electronics to customizable health monitoring devices. We believe that the fundamental framework for subtractive printing, which incorporates etching and storage of materials in a reservoir that can be subsequently removed is generalizable, and will open up new directions in subtractive manufacturing that can overcome the challenges of direct printing with inks that would otherwise evaporate in an uncontrolled manner.

4. Experimental Section

Atomic Layer Deposition: A custom-built, hot wall, cross-flow thermal ALD reactor was used to deposit zinc oxide (ZnO) onto silicon substrates at a temperature of 130 °C. Diethylzinc (DEZ, Sigma-Aldrich, St. Louis, MO, ≥52 wt% Zn bases) was used as the metalorganic precursor, deionized water (DI water) as the oxidant, and argon (Ar) as the carrier gas at 70 s ccm. For the ZnO deposition cycle, DEZ was pulsed for 0.05 s, then purged for 30 s, and DI water was pulsed for 0.1 s, then purged for 30 s. The average growth rate on the silicon wafer piece was measured to be 2 Å $cycle^{-1}$ using spectroscopic ellipsometry.

Electrohydrodynamic Jet Printing: The e-jet printer system used for the experiments was custom-built within the Barton Research Group at the University of Michigan.[10] This system includes an x-y-z nano-positioning stage, a voltage amplifier, a camera, a light source for nozzle distance adjustments and jetting visualization with 10x magnification lensing, and a nozzle holder. The nozzles were pre-pulled glass micropipettes with a 10 µm opening purchased from World Precision Instruments (WPI). 1 M HCl was mixed with 2 wt.% of glycerol as the ink unless stated otherwise. The nozzle offset from the substrate was set to be 30 µm. A DC voltage signal for the e-jetting process with a voltage of 680 V was used and the printing speed was fixed at 0.01 mms^{-1}. More detailed information on e-jet parameters is summarized below in Table S3 (Supporting Information).

Material Characterization: Spectroscopic ellipsometry was performed with a J. A. Woollam M-2000 ellipsometer using a Cauchy model to measure the thickness of ALD films. Optical microscopy images were taken using Keyence VHX-7000 Digital Microscope. Atomic Force Microscopy (AFM) was performed with a MFP-3D Origin+ AFM from Asylum Research. Scanning Electron Microscopy (SEM) images were taken using a FEI Helios G4 Plasma FIB UXe. Elemental mapping was performed using energy-dispersive X-ray spectroscopy (EDS) with an accelerating voltage of 10 kV. Owing to the high voltage requirement for EDS of Zn, elemental mapping of the residual polymer composite before removal was performed on a larger printed droplet to minimize effects from beam damage.

Supporting Information

Supporting Information is available from the Wiley Online Library or from the author.

Acknowledgements

T.H.C. and N.F. contributed equally to this work. This material was based upon work supported by the National Science Foundation under Grants No. 1727918 and 1751590. Portions of this work were performed at the Michigan Center for Materials Characterization, which was supported by the College of Engineering at the University of Michigan.

Conflict of Interest

The authors declare no conflict of interest.

Data Availability Statement

The data that support the findings of this study are available from the corresponding author upon reasonable request.

Keywords

3-D printing, additive manufacturing, atomic layer deposition, printable devices, subtractive patterning

Received: October 13, 2023
Revised: December 16, 2023
Published online: December 31, 2023

[1] D. S. Engstrom, B. Porter, M. Pacios, H. Bhaskaran, *J. Mater. Res.* **2014**, *29*, 1792.
[2] A. Zhakeyev, P. Wang, L.i Zhang, W. Shu, H. Wang, J. Xuan, *Adv. Sci.* **2017**, *4*, 1700187.
[3] J. A. Liddle, G. M. Gallatin, *ACS Nano* **2016**, *10*, 2995.
[4] R. D. Farahani, M. Dubé, D. Therriault, *Adv. Mater.* **2016**, *28*, 5794.
[5] Y.-L. Zhang, Q.-D. Chen, H. Xia, H.-B. Sun, *Nano Today* **2010**, *5*, 435.
[6] M. Deubel, G. Von Freymann, M. Wegener, S. Pereira, K. Busch, C. M. Soukoulis, *Nat. Mater.* **2004**, *3*, 444.
[7] R. D. Piner, J. Zhu, F. Xu, S. Hong, **1999**, *283*, 661.
[8] E. DM, S. EK, *Nature* **1990**, *344*, 524.
[9] J.-U. Park, M. Hardy, S. J. Kang, K. Barton, K. Adair, D. K. Mukhopadhyay, C. Y. Lee, M. S. Strano, A. G. Alleyne, J. G. Georgiadis, P. M. Ferreira, J. A. Rogers, *Nat. Mater.* **2007**, *6*, 782.
[10] C. P. Pannier, L. Ojeda, Z. Wang, D. Hoelzle, K. Barton, *Mechatronics* **2018**, *56*, 268.
[11] M. S. Onses, E. Sutanto, P. M. Ferreira, A. G. Alleyne, J. A. Rogers, *Small* **2015**, *11*, 4237.
[12] N. Mkhize, H. Bhaskaran, *Small Science* **2022**, *2*, 2100073.
[13] S. Su, J. Liang, Z. Wang, W. Xin, X. Li, D. Wang, *Nanoscale* **2020**, *12*, 24450.
[14] Y. Ding, C. Zhu, J. Liu, Y. Duan, Z. Yi, J. Xiao, S. Wang, Y. Huang, Z. Yin, *Nanoscale* **2017**, *9*, 19050.
[15] S. Lee, J. Kim, J. Choi, H. Park, J. Ha, Y. Kim, J. A. Rogers, U. Paik, *Appl. Phys. Lett.* **2012**, *100*, 102108.
[16] Y. G. Lee, W.-S. Choi, *ACS Appl. Mater. Interfaces* **2014**, *6*, 11167.
[17] B. H. Kim, M. S. Onses, J. B. Lim, S. Nam, N. Oh, H. Kim, K. J. Yu, J. W. Lee, J.-H. Kim, S.-K. Kang, C. H. Lee, J. Lee, J. H.o Shin, N. H. Kim, C. Leal, M. Shim, J. A. Rogers, *Nano Lett.* **2015**, *15*, 969.
[18] K. Kim, G. Kim, B. R. Lee, S. Ji, S.-Y. Kim, B. W. An, M. H. Song, J.-U. Park, *Nanoscale* **2015**, *7*, 13410.
[19] H.-J. Kwon, J. Hong, S. Y. Nam, H. H. Choi, X. Li, Y. J. Jeong, S. H. Kim, *Mater Adv* **2021**, *2*, 5593.
[20] Z. Afkhami, B. Iezzi, D. Hoelzle, M. Shtein, K. Barton, *Adv. Mater. Technol.* **2020**, *5*, 1.
[21] D. H. Levy, C. R. Ellinger, S. F. Nelson, *Appl. Phys. Lett.* **2013**, *103*, 043505.
[22] S. F. Nelson, C. R. Ellinger, D. H. Levy, *ACS Appl. Mater. Interfaces* **2015**, *7*, 2754.
[23] T. H. Cho, N. Farjam, C. R. Allemang, C. P. Pannier, E. Kazyak, C. Huber, M. Rose, O. Trejo, R. L. Peterson, K. Barton, N. P. Dasgupta, *ACS Nano* **2020**, *14*, 17262.
[24] B. A. Rorem, T. H. Cho, N. Farjam, J. D. Lenef, K. Barton, N. P. Dasgupta, L. J. Guo, *ACS Appl. Mater. Interfaces* **2022**, *14*, 31099.

[25] D. Gao, J. G. Zhou, *Int. J. Bioprint.* **2019**, *5*, 1.
[26] Z. Xu, H. qun Zou, J. Wang, M. qi Zhang, D. zhi Wang, J. shan Liu, *Microsyst. Technol.* **2018**, *24*, 1207.
[27] W. Zou, H. Yu, P. Zhou, Y. Zhong, Y. Wang, L. Liu, *Appl. Surf. Sci.* **2021**, *543*, 148800.
[28] M. G. Steven, *Chem. Rev.* **2010**, *110*, 111.
[29] M. J. Biercuk, D. J. Monsma, C. M. Marcus, J. S. Becker, R. G. Gordon, *Appl. Phys. Lett.* **2003**, *83*, 2405.
[30] A. J. M. Mackus, J. R. Schneider, C. Macisaac, J. G. Baker, S. F. Bent, *Chem. Mater.* **2019**, *31*, 1142.
[31] N. P. Dasgupta, H.-B.-R. Lee, S. F. Bent, P. S. Weiss, *Chem. Mater.* **2016**, *28*, 1943.
[32] N. Farjam, T. H. Cho, N. P. Dasgupta, K. Barton, *Appl. Phys. Lett.* **2020**, *117*, 133702.
[33] E. Färm, M. Kemell, E. Santala, M. Ritala, M. Leskelä, *J. Electrochem. Soc.* **2009**, *157*, K10.
[34] G. N. Parsons, R. D. Clark, *Chem. Mater.* **2020**, *32*, 4920.
[35] A. Mameli, B. Karasulu, M. A. Verheijen, A. J. M. Mackus, W. M. M. Kessels, F. Roozeboom, *ECS Trans.* **2017**, *80*, 39.
[36] A. J. M. Mackus, M. J. M. Merkx, W. M. M. Kessels, **2019**, *31*, 2.
[37] S. Stefanovic, N. Gheshlaghi, D. Zanders, I. Kundrata, B. Zhao, M. K. S. Barr, M. Halik, A. Devi, J. Bachmann, *Small* **2023**, *19*, 2301774.
[38] I. Kundrata, M. K. S. Barr, S. Tymek, D. Döhler, B. Hudec, P. Brüner, G. Vanko, M. Precner, T. Yokosawa, E. Spiecker, M. Plakhotnyuk, K. Fröhlich, J. Bachmann, *Small Methods* **2022**, *6*, 2101546.
[39] N. P. Dasgupta, J. Sun, C. Liu, S. Brittman, S. C. Andrews, J. Lim, H. Gao, R. Yan, P. Yang, *Adv. Mater.* **2014**, *26*, 2137.
[40] T. Tynell, M. Karppinen, *Semicond. Sci. Technol.* **2014**, 043001, *29*,.
[41] A. Di Mauro, M. E. Fragalà, V. Privitera, G. Impellizzeri, *Mater. Sci. Semicond. Process.* **2017**, *69*, 44.
[42] H. Maki, T. Ikoma, I. Sakaguchi, N. Ohashi, H. Haneda, J. Tanaka, N. Ichinose, *Thin Solid Films* **2002**, *411*, 91.
[43] S. J. Pearton, D. P. Norton, K. Ip, Y. W. Heo, T. Steiner, *Superlattices Microstruct.* **2003**, *34*, 3.
[44] C. P. Pannier, M. Diagne, I. A. Spiegel, D. J. Hoelzle, K. Barton, *J. Manuf. Sci. Eng.* **2017**, *139*, 111008.
[45] A. Bahrami, A. Hawa, K. Yue, K. Barton, 2023 IEEE Conference on Control Technology and Applications (CCTA) August **2023**, 143.
[46] N.-S. Cheng, *Ind. Eng. Chem. Res.* **2008**, *47*, 3285.
[47] N. Farjam, I. A. Spiegel, K. Barton, *Materialia (Oxf)* **2022**, *26*, 101578.
[48] H. Hu, R. G. Larson, *J. Phys. Chem. B* **2006**, *110*, 7090.
[49] M. Majumder, C. S. Rendall, J. A. Eukel, J. Y. L. Wang, N. Behabtu, C. L. Pint, T.-Y. Liu, A. W. Orbaek, F. Mirri, J. Nam, A. R. Barron, R. H. Hauge, H. K. Schmidt, M. Pasquali, *J. Phys. Chem. B* **2012**, *116*, 6536.
[50] J. R. Mileham, S. J. Pearton, C. R. Abernathy, J. D. Mackenzie, R. J. Shul, S. P. Kilcoyne, *Appl. Phys. Lett.* **1995**, *67*, 1119.
[51] P. Candeloro, E. Comini, C. Baratto, G. Faglia, G. Sberveglieri, R. Kumar, A. Carpentiero, E. Di Fabrizio, *J. Vac. Sci. Technol. B* **2005**, *23*, 2784.